Title

Methylation at the C-2 position of hopanoids increases rigidity in native bacterial membranes

Authors and Affiliations

Chia-Hung Wu[a,c], Maja Bialecka-Fornal[a], and Dianne K. Newman[a,b,c,1]

[a]Division of Biology and Biological Engineering, California Institute of Technology, Pasadena, California, USA

[b]Division of Geological and Planetary Sciences, California Institute of Technology, Pasadena, California, USA

[c]Howard Hughes Medical Institute, Pasadena, California, USA

[1] To whom correspondence should be addressed: dkn@caltech.edu

Contributions

CHW, MB-F, DKN: Conception and design, Analysis and interpretation of data, Drafting or revising the article. CHW, MB-F: Acquisition of data/

Abstract

Sedimentary rocks host a vast reservoir of organic carbon, such as 2-methylhopane biomarkers, whose evolutionary significance we poorly understand. Our ability to interpret this molecular fossil record is constrained by ignorance of the function of their molecular antecedents. To gain insight into the meaning of 2-methylhopanes, we quantified the dominant (des)methylated hopanoid species in the membranes of the model hopanoid-producing bacterium *Rhodopseudomonas palustris* TIE-1. Fluorescence polarization studies of small unilamellar vesicles revealed that hopanoid 2-methylation specifically renders native bacterial membranes more rigid at concentrations that are relevant *in vivo*. That hopanoids differentially modify native membrane rigidity as a function of their methylation state indicates that methylation itself promotes fitness under stress. Moreover, knowing the *in vivo* (2Me)-hopanoid concentration range in different cell membranes, and appreciating that (2Me)-hopanoids' biophysical effects are tuned by the lipid environment, permits the design of more relevant *in vitro* experiments to study their physiological functions.

Introduction

Lipids play essential roles in compartmentalizing cells for specific functions and creating barriers that are selectively permeable to the environment. The composition of lipids in cell membranes varies significantly and the basic biophysical properties of membranes, such as rigidity and permeability, can be adjusted based on growth conditions and environmental stressors (Lipowsky & Sackmann, 1995 ; Los & Murata, 2004 ; Neubauer et al., 2014). One well-studied example is cholesterol in eukaryotic membranes. This essential sterol plays diverse roles in maintaining membrane structural integrity, modifying membrane rigidity, serving as a biosynthetic precursor for steroid hormones, vitamin D, and bile acids, or acting as a protein modifier for signaling pathways (Gallet, 2011 ; Hanukoglu, 1992 ; Song et al., 2014). In addition to their important biological functions, lipids are of interest because they are more geostable than other biomolecules. For example, hopanoid molecular fossils, “hopanes”, date back over a billion years (Brocks et al., 2005), and are so abundant that the global stock of hopanoids that can be extracted from sedimentary rocks is estimated to be 10^{13} or 10^{14} tons, more than the estimated 10^{12} tons of organic carbon in all living organisms (Ourisson et al., 1984). In contrast to steroids, hopanoids are a less well-studied but evolutionarily significant and chemically diverse class of lipids that are thought to be sterol surrogates in bacteria (Figure 1) (Rohmer et al., 1979 ; Ourisson et al., 1987).

60 The rich record of ancient lipids, including fossil hopanoids, has long been
61 recognized to hold clues into the early history of life and past environments
62 (Ourisson et al., 1984 ; Summons & Walter, 1990 ; Brocks & Pearson, 2005 ;
63 Knoll et al., 2007). But being able to confidently interpret the meaning of any
64 ancient molecular fossil poses considerable challenges. First, we must be able
65 to identify potential sources for these compounds, demanding unambiguous
66 chemical parity between modern and ancient structures. Once this is achieved,
67 understanding whether particular environmental conditions regulate the
68 production of specific hopanoid variants becomes important. But arguably the
69 most critical goal in advancing our understanding of ancient lipids, is being able
70 to identify specific biological functions for their counterparts in cells today.
71 Myriad hopanoid structures are known to exist (Ourisson et al., 1984), yet we
72 only poorly understand the significance of this chemical diversity. For meaningful
73 linkages to be made between modern compounds and ancient biomarkers, we
74 must: 1.) study those hopanoids that leave a specific trace in sedimentary rocks
75 (*e.g.* their chemical modifications are geostable), 2.) identify their *in vivo*
76 function(s) and 3.) evaluate whether the roles played by these lipids in modern
77 organisms have been conserved over the course of evolution.

78 Following the recognition in the early 1970s that hopanes are ubiquitous in
79 sedimentary rocks, the occurrence of hopanoids in diverse organisms was
80 documented, and insights were gained into their biosynthesis, biophysical
81 properties, and cellular functions (Ourisson et al., 1987 ; Ourisson & Rohmer,

1992 ; Pearson, 2013). For example, studies using hopanoid-deficient mutants have shown that hopanoids promote resistance to antibiotics, detergents, extreme pH, and high osmolarity (Schmerk et al., 2011 ; Malott et al., 2012 ; Sáenz, 2010 ; Welander et al., 2009 ; Kulkarni et al., 2013). Biophysical studies using mixtures of hopanoids and model lipids have demonstrated that, like cholesterol, bacteriohopanetetrol cyclitol ether can condense membranes at high temperatures but fluidize membranes at low temperatures (Poralla et al., 1980). Similarly, bacteriohopanetetrol (BHT) and bacteriohopanemonol can condense model membranes, and diplopterol (Dip) can form liquid ordered microdomains (Kannenberg et al., 1983 ; Nagumo et al., 1991 ; Ourisson & Rohmer, 1992 ; Sáenz et al., 2012). A recent molecular modeling study pointed out different behaviors between Dip and BHT in their specific location within lipid bilayers and their capacity to condense membranes, suggesting complex roles of hopanoids due to their structural diversity (Poger & Mark, 2013). These biophysical studies have provided insights into the physical capabilities of these hopanoids. However, whether hopanoids play the same roles *in vivo* has been unclear due to the differences in lipid composition and concentration between model and cellular membranes.

Among various hopanoid modifications, methylation of C-2 on the A-ring has drawn attention from Earth scientists because this modification is preserved episodically in ancient sedimentary rocks dating back to 1.6 billion years ago; accordingly, it has been suggested that 2-methylated hopanes (2Me-hopanes),

104 the molecular fossils of 2Me-hopanoids, could potentially serve as biomarkers to
105 interpret events in the early history of life (Brocks et al., 2005 ; Rasmussen et al.,
106 2008). For a time, it was thought that 2Me-hopanes were biomarkers of
107 cyanobacteria, and hence the process of oxygenic photosynthesis (Summons et
108 al., 1999), but we now know this not to be the case (Welander et al., 2010 ; Ricci
109 et al., 2015). Intriguingly, spikes in the C_{30} 2-Me hopane index (ratio of
110 methylated short hopanes to total short hopanes) through geologic time are
111 correlated with episodes of oceanic anoxic events (OAEs), which are thought to
112 have imposed heightened stress on the biosphere (Knoll et al., 2007).

113 Towards the goal of finding a robust interpretation for 2Me-hopanes, we
114 have elucidated the biosynthetic pathway of 2Me-hopanoids (Welander et al.,
115 2010 ; Welander et al., 2012), linked 2Me-hopanoids to specific environments
116 and producers through (meta)genomic studies (Ricci et al., 2014), and identified
117 the stress-responsive pathway regulating transcription of the 2-methylase (*hpnP*)
118 in the model hopanoid-producing bacterium *Rhodospeudomonas palustris* TIE-1
119 (Kulkarni et al., 2013). A major challenge in understanding the function of 2Me-
120 hopanoids has been the lack of a clear phenotype *in vivo,* despite dedicated
121 attempts to find one for the *hpnP* mutant (Kulkarni et al., 2013). Recent data
122 suggest this phenotypic silence results from changes to the lipidome that
123 compensate for the loss of 2Me-hopanoids (Neubauer et al., 2014). To infer a
124 specific *in vivo* function for 2Me-hopanoids, *in vitro* studies that mimic cellular
125 composition are therefore necessary.

126 We hypothesized that methylation at C-2 would change hopanoids'
127 packing with other lipids and proteins and affect membrane biophysical
128 properties such as rigidity. Furthermore, we reasoned that such an effect would
129 depend on the specific lipid composition of the membrane. To test these
130 hypotheses, we took advantage of the existence of specific hopanoid-mutant
131 strains (Welander et al., 2010 ; Welander et al., 2012), and recently developed
132 protocols allowing quantitative analysis and the purification of hopanoids and
133 their 2-methylated species in large quantities (Wu et al., 2014). This
134 experimental foundation set the stage for what we now report: *in vitro* membrane
135 studies to examine how 2Me-hopanoids affect membrane rigidity in the context of
136 different lipid environments of relevance to the cell. Our finding that hopanoid
137 methylation enhances membrane rigidity supports the interpretation that past
138 intervals of heightened 2Me-hopane abundance record a history of stress.

139

140 **Results**

141 **Whole cell membrane fluidity.**

142 To test whether 2-methylation changes membrane rigidity, we measured the
143 membrane rigidity of specific hopanoid biosynthetic mutants (Table 1) (Welander
144 et al., 2012) using fluorescence polarization. Figure 2 shows the whole cell
145 membrane rigidity measured at 25 °C and 40 °C. As expected, at higher
146 temperature, the cell membrane became less rigid across all strains. At 25 °C,

147 the Δ*shc* mutant, which lacks all hopanoids, had the least rigid membrane. This
148 could be caused by both the absence of hopanoids and the accumulation of the
149 hopanoid biosynthetic precursor, squalene. The result is also consistent with the
150 observation that in model lipid vesicles, hopanoids make the membrane more
151 rigid (Kannenberg et al., 1985). Interestingly, the production of only short-chain
152 hopanoids (Δ*hpnH*) is sufficient to recover the rigidity level close to that of the
153 WT. However, when an adenosine molecule is attached to short hopanoids and
154 accumulates in the Δ*hpnG* mutant, rigidity decreases to Δ*shc* levels. Furthermore,
155 in Δ*hpnN* where hopanoids are unable to be transported to the outer membrane
156 (Doughty et al., 2011), membrane rigidity is similar to Δ*hpnG*. These results have
157 two implications. First, the hydrophobic reporter dye we used for fluorescence
158 polarization measurements, diphenyl hexatriene (DPH), reflects mostly the
159 rigidity of the outer membrane. Second, the types of hopanoids and their
160 respective localization between the inner and outer membranes directly impact
161 membrane rigidity.

162 Interestingly, no obvious impact on rigidity was found in the absence of
163 either bacteriohopane aminotriol (Δ*hpnO*) or 2-methylhopanoid (Δ*hpnP*) or both
164 (Δ*hpnOP*) compared to WT (Figure 2). This observation could have two possible
165 explanations. One is that these specific hopanoids do not affect membrane
166 rigidity in cells. The other explanation is that the cells might synthesize other
167 lipids that compensate for their effects so that no phenotype is observed. We can
168 distinguish between these two scenarios by measuring membrane rigidity using

vesicles made of model lipids and purified hopanoids. However, to design experiments that are physiologically relevant, we first needed to quantify hopanoids distribution in both the inner (IM) and outer membrane (OM) of *R. palustris* TIE-1.

Quantification of hopanoids in the inner and outer membranes of *R. palustris* TIE-1.

It is well appreciated that lipids can have different subcellular localization, even in bacteria (Matsumoto et al., 2006). To understand the biological roles of hopanoids, especially for 2-methylhopanoids, we measured the amounts of different hopanoids in the IM and OM of *R. palustris* TIE-1 WT and Δ*hpnP* using a previously described protocol (Figure 3) (Morein et al., 1994 ; Wu et al., 2014 ; Neubauer et al., 2014). Table 2 shows that the total yield of the fractionated membranes was about 10% weight of dried cells, which is comparable to 9.1% in *E. coli* (Neidhardt & Curtiss, 1996). The yields of the total lipid extract (TLE) from the lyophilized fractionated membranes were ~12-15% from the IM and ~5% for the OM. This yield is reproducible and could be due to a larger proportion of membrane proteins in *R. palustris* TIE-1, lower recovery after lyophilization, or loss of certain lipid classes that were not quantitatively extracted by procedures optimized for hopanoids. The TLE yield in the OM was at least 50% lower than that in the IM, which is expected because the outer leaflet of the OM consists of

more hydrophilic lipid A and lipopolysaccharides that are not extractable by the hydrophobic Bligh-Dyer lipid extraction method we employed.

To quantify hopanoids, TLE from IM and OM were analyzed by GC-MS using androsterone as an internal standard and the differences in ionization efficiencies between androsterone and hopanoids were calibrated by external standards using purified hopanoids (Figure 3). Such calibration was recently shown to be essential for accurate hopanoid quantification (Wu et al., 2014). Using this approach, the exact weight% of each hopanoid in TLE was obtained. However, to put the numbers in context and compare the value in mol%, we assumed the average molecular weight of the total lipids is 786 g/mol, the same as dioleoyl phosphatidylcholine (DOPC) and *E. coli* polar lipid extract (PLE). Because we could only confidently quantify (2Me)-Dip and (2Me)-BHT, we focused our analyses on these four hopanoids. Figure 4 shows the hopanoid quantification results. In both WT and Δ*hpnP*, each type of hopanoid is enriched in the OM compared to the IM. The total of these four hopanoids in the IM is ~2.6 mol% of TLE, whereas in the OM, the value can reach 8-11 mol%. For individual hopanoids in WT, the mol% in IM and OM are 1% and 2% for Dip, 1% and 2.4% for 2Me-Dip, 0.4% and 3.4% for BHT, and 0.1% and 0.3% for 2Me-BHT, respectively. In Δ*hpnP*, the IM and OM values are 2% and 7.5% for Dip, and 0.5% and 4.3% for BHT, respectively (Figure 4). This quantitative measurement of hopanoid content within the IM and OM can be used to evaluate the impact of 2-methylation upon hopanoid subcellular distribution.

The ratio of total hopanoids in the OM versus IM is 3.1±0.4 and 4.4±0.6 for WT and Δ*hpnP*, respectively, which is a significant difference (P=0.038). Comparing the ratios between short ((2Me)-Dip) and long ((2Me)-BHT) chain hopanoids revealed an enrichment of long-chain hopanoids in the OM compared to the IM in both WT and Δ*hpnP* (Figure 5). Interestingly, about equal amounts of 2Me-Dip and Dip were found in both IM and OM, whereas 2Me-BHT is 16% and 8% of BHT in the IM and OM, respectively, suggesting hopanoid 2-methylation has neither strong nor consistent effects on the partitioning of short and long species between the IM and OM (Figure 5). However, our data does indicate that 2-methylation impacts that total amount of hopanoid enrichment in the OM.

Membrane rigidity measurements using model lipid SUVs.

To put these numbers in context and gain a deeper understanding on how the amount, chain-length, and 2-methylation of hopanoids impact membrane biophysical properties, we performed membrane rigidity measurements. Small unilamellar vesicles (SUVs) are commonly used for such measurements because it is straightforward to control their lipid composition (Hope et al., 1985). We used fluorescence polarization to measure the fluorescence of DPH, a reporter dye, in the presence of model lipids and purified hopanoids. Figure 6 shows how the membrane rigidity of model lipids, DOPC and *E. coli* PLE, responds to the presence of cholesterol, squalene, (2Me)-Dip, and (2Me)-BHT. Because the total

hopanoids in cell membranes are ~10 mol% (Figure 4), we varied the concentration of hopanoids between 5 to 20 mol% in SUVs, which our quantification results suggest are physiologically relevant concentrations. Starting with the simplest single lipid background, DOPC, the addition of cholesterol increases membrane rigidity and the magnitude of change is proportional to the amounts of cholesterol added (black line, Figure 6A). This observation is consistent with the literature and validates our technical approach (Vanblitterswijk et al., 1987). Interestingly, the addition of the hopanoid precursor, squalene, has the opposite effect as cholesterol and makes the membrane less rigid in a concentration dependent fashion (magenta line, Figure 6A). However, when Dip is added, the membrane rigidity is unaffected (dark blue line, Figure 6A). Surprisingly, given the structural similarity between cholesterol and Dip, Dip does not seem to rigidify DOPC as extensively as does cholesterol. However, when Dip is further processed by the cell to produce BHT, it rigidifies DOPC vesicles in the same manner as cholesterol (red line, Figure 6A).

2-methylation of both Dip and BHT has striking effects on their ability to rigidify DOPC. Not only does 2-methylation increase DOPC membrane rigidity, but at 20 mol%, 2Me-Dip even outperforms cholesterol and BHT (light blue, Figure 6A). 2Me-BHT also increases membrane rigidity similar to cholesterol, even though the difference from BHT is much smaller than that between Dip and 2Me-Dip (orange line, Figure 6A). This result demonstrates methylation itself changes the biophysical properties of hopanoids, which directly impacts

membrane fluidity. This observation reinforces the interpretation that the lack of phenotype in the Δ*hpnP* strain may be due to cells synthesizing other lipids that functionally complement the absence of 2Me-hopanoids, rather than due to a lack of an impact at the molecular level *per se*.

To determine whether the effects on membrane rigidity by these hopanoids hold in more physiologically relevant environments, we repeated the experiment using *E. coli* PLE as the main component to form SUVs (Figure 6B). *E. coli* PLE from Avanti Polar Lipids consists of 67% phosphatidylethanolamine (PE), 23.2% phosphatidylglycerol (PG), and 9.8% cardiolipin (CL) (in weight %), and has an average molecular weight identical to DOPC (786 g/mol). Compared to DOPC alone, the SUVs from *E. coli* PLE are more rigid, probably because the difference in fatty acid chain saturation (green square, Figure 6A and 6B). Even though *E. coli* PLE SUVs are more rigid than DOPC SUVs to start with, we observe the same trend, where adding cholesterol rigidifies the vesicles, and squalene fluidizes them. However, the concentration dependence on the rigidity change is more dramatic for cholesterol compared to squalene (black line, Figure 6B). Unlike in DOPC, Dip has a small rigidifying effect in the *E. coli* PLE background, yet similar to DOPC, no concentration dependence is observed (blue line, Figure 6B).

Addition of 2Me-Dip also rigidifies *E. coli* PLE, but in contrast to what was observed for DOPC, 2Me-Dip shows lower capacity to rigidify the membrane than cholesterol (cyan line, Figure 6B). Interestingly, the extended hopanoid,

277 BHT, also rigidifies the membrane, but seemed to saturate at 10 mol% (red line,
278 Figure 6B). Surprisingly, in sharp contrast to the DOPC background, 2Me-BHT
279 strongly rigidifies the *E. coli* PLE membranes and has a concentration
280 dependence (orange line, Figure 6B). This result shows that the impact of 2-
281 methylation and hopanoid extension on a membrane biophysical property
282 depends on the specific lipid environment. As expected, when these experiments
283 were repeated at 40 °C, membranes were less rigid overall. However, similar
284 trends compared to 25 °C were observed in both DOPC and *E. coli* PLE
285 background (Figure 6-figure supplement 1).

286

287 **Quantification of phospholipid composition in *R. palustris* TIE-1.**

288 Given that 2-methylation of hopanoids differentially impacts membrane rigidity
289 based on the lipid context, to understand the physiological effects of 2-
290 methylhopanoids in the IM and OM of *R. palustris* TIE-1, we must characterize
291 the composition of phospholipids in native membranes and perform biophysical
292 experiments using these membranes. To determine the exact quantity of each
293 phospholipid in *R. palustris* TIE-1, we purified the IM and OM as described above
294 and analyzed the lipid composition by LC-MS using electron spray ionization
295 (Neubauer et al., 2014 ; Malott et al., 2014). The elution profiles between strains
296 and membranes look similar (Figure 7). A total of 33 major phospholipids were
297 identified, including 10 PC, 9 PE, 7 PG, and 7 CL (Table 3). To determine the

298 absolute quantity of each phospholipid, exogenous standards of PC (17:0/17:0),
299 PE (17:0/17:0), and PG (17:0/17:0) that are absent in *R. palustris* TIE-1 were
300 added as internal standards for LC-MS analyses. Although we can detect
301 cardiolipins, we unfortunately are unable to quantify them due to the low solubility
302 of the cardiolipin standard in the LC-MS solvent.

303 Table 4 shows the weight% of each identified phospholipid in the TLE.
304 Among the identified phospholipids, the IM in WT and Δ*hpnP* has ~50%, ~36%,
305 and ~12-14% of PC, PE, and PG, respectively, whereas the OM in WT and
306 Δ*hpnP* has ~56-58%, ~30-33%, and ~11-12% of PC, PE, and PG, respectively.
307 However, when we calculate the total identified phospholipid amount, it only
308 accounts for ~26-34 weight% of the original TLE samples (Table 4). This low
309 value could be due to 1) low solubility of cardiolipins and other unidentifiable
310 lipids in LC-MS, 2) differences in the ionization efficiency of the phospholipids
311 with different chain length or saturation (Myers et al., 2011), and 3) the ionization
312 suppression effects occur from co-eluting lipids (Brugger et al., 1997 ; Furey et
313 al., 2013). Nevertheless, the average molecular weight of the phospholipids
314 without cardiolipin is 738 g/mol. Considering the higher molecular weight of
315 cardiolipin, our calculation for the mol% of hopanoids in TLE using an average
316 molecular weight of 786 g/mol may be very close to the real value in *R. palustris*
317 TIE-1.

318

Membrane rigidity measurements using lipid extract from *R. palustris* TIE-1 inner and outer membranes.

Due to the limitations we encountered in quantifying native phospholipids, we elected to generate SUVs directly using the TLE from fractionated *R. palustris* TIE-1 IM and OM rather than reconstituting SUVs from commercially available sources. Because our main focus is on the effect of 2-methylhopanoids, we used the membranes from Δ*hpnP* and added 5, 10, and 20 mol% purified hopanoids to constitute the SUV lipid mixture. We also included WT IM and OM for comparison. Figure 8 shows membrane rigidity measurements at 25 °C using *R. palustris* TIE-1 membranes. In both WT and Δ*hpnP*, the OM showed higher membrane rigidity than IM, which could be due to the higher hopanoid content in the OM (Figure 4) and differences in phospholipid content. Compared to WT, the Δ*hpnP* IM and OM showed decreased rigidity. This contrasts with our whole cell membrane rigidity results in which no difference in rigidity was observed (Figure 2). This discrepancy could be due to the presence of lipid A and outer membrane proteins that may affect the overall membrane rigidity in whole cells.

Similar to our observations in model lipids, the addition of Dip has no effect on membrane rigidity, both in the IM and OM. However, 2Me-Dip rigidifies both IM and OM in a concentration dependent manner, as seen in the model lipid SUVs. Interestingly, unlike the effects BHT exerts in model lipids, it does not rigidify either the IM or OM. While it is possible that BHT has no effect on native

membrane rigidity, given that Δ*hpnP* membranes contain BHT, it seems more likely that endogenous BHT is saturating its membrane rigidifying capacity, similar to what we observed for *E. coli* PLE (red line, Figure 6B).

When BHT is methylated, it rigidifies both the IM and OM. However, different trends can be seen between these membranes: in the IM, the more 2Me-BHT present, the higher the membrane rigidity, yet OM membrane rigidity appears to saturate by 5 mol% 2Me-BHT and remains constant between 5-20 mol% of 2Me-BHT (Figure 8B). It is tempting to speculate that the reason less 2-methylation occurs for BHT than Dip in the OM (Figure 4, 5) is because less methylation of BHT is needed to significantly impact OM rigidity.

We repeated these experiments at 40 °C and observed similar trends as seen at 25 °C (Figure 8-figure supplement 1). However, we had larger standard deviations than in our model lipid experiments, which could be due to higher heterogeneity in the samples extracted from IM and OM. Nevertheless, we find clear physiologically relevant distinctions in the rigidifying effects of both short and long 2Me-hopanoids on the IM and OM of *R. palustris* TIE-1.

Discussion

Until now, a specific role for 2Me-hopanoids in living cells has evaded experimental detection, yet its identification has been of great interest for

360 interpreting the extensive 2Me-hopane fossil record (Welander et al., 2010 ;
361 Kulkarni et al., 2013). Our findings that 2Me-hopanoids rigidify membranes to
362 different extents depending both on their specific structure (short or long) and
363 lipid context not only provide a clear biological function for these compounds, but
364 also help rationalize why previous efforts to identify such a function have been
365 challenging. That methylation *per se* can contribute to rigidifying membranes
366 may also help explain the association of methylated hopanoids in certain modern
367 and ancient environments.

368 Under what circumstances would adding a methyl group at the 2' position
369 of hopanoids, which seems a rather small modification, be beneficial? Might
370 there be a mechanistic explanation for the enrichment of 2-Me hopanes during
371 stressful OAEs (Knoll et al., 2007)? Several independent lines of evidence bridge
372 our biophysical findings with the abundance patterns in the rock record, together
373 suggesting that 2-methylhopanoids confer stress resistance: 1.) 2-Me hopanoids
374 are enriched in the outer membrane of akinetes, survival cell types of the
375 cyanobacterium *Nostoc punctiforme* (Doughty et al, 2009), 2.) a stress-
376 responsive pathway upregulates the HpnP methylase in *R. palusris* (Kulkarni et
377 al., 2013), 3.) in modern environments, the capacity for 2Me-hopanoid production
378 significantly correlates with organisms, metabolisms (*e.g.* nitrogen fixation) and
379 environments that support plant-microbe interactions (Ricci et al., 2014). This
380 correlation, together with the observation that (2Me)-hopanoids promote
381 symbiosis (Silipo et al., 2014), tempt us to speculate that 2Me-hopanoids may

382 indirectly facilitate nitrogen fixation by enhancing bacterial survival under the
383 stressful conditions that accompany the establishment of symbiosis (Gibson et al,
384 2008). Going forward, it is worth critically examining this hypothesis; if correct,
385 such an interpretation would indicate that spikes in the 2Me-hopane index may
386 reflect episodes of particular environmental stresses favoring the growth of
387 organisms capable of withstanding it using (2Me)-hopanoids.

388 How might the 2-methylation of hopanoids permit such an adventitious
389 adaptation? Molecular dynamic simulations of 2Me-hopanoid within a relevant
390 lipid context are required to understand the interactions on an atomic scale.
391 However, we may speculate about the mechanism of rigidification through
392 lessons learned from studies of cholesterol, in which the number of methyl
393 groups control its optimal molecular packing to geometrically complement
394 phospholipid chains (Bloch, 1979). The addition or removal of methyl groups over
395 the evolution of the cholesterol lipid family is thought to have optimally tuned
396 cholesterol's ability to order or condense phospholipid membranes (Miao et al.,
397 2002 ; Rog et al., 2007). We suggest that when a methyl group is added onto
398 the 2' position of A-ring in hopanoid, the stearic hindrance between the 2-methyl
399 group and the methyl groups at the 4' and 10' position of the A-ring could
400 transform the ring from a chair to a twisted conformation. The two additional 1,3-
401 diaxial interactions elicited by hopanoid 2-methylation could mimic the smoothing
402 and/or tilting effect known for cholesterol, thus rationalizing how 2-methylation
403 may improve the ability of hopanoids to rigidify membranes (Rog et al., 2007).

404 The differences in (2Me)-hopanoid distribution between the IM and OM
405 pose many interesting questions about their role in maintaining membrane
406 integrity and homeostasis. Compared to (2Me)-Dip, the addition of a hydrophilic
407 tail to form (2Me)-BHT or even BHT-glucosamine (Figure 1) may favor a stronger
408 interaction with the outer leaflet of the OM, in which the lipid head group is
409 heavily modified with hydrophilic molecules. The relative enrichment of (2Me)-
410 BHT in the OM is consistent with such a scenario. The hydrophilic tail of 2Me-
411 BHT could also affect the vertical position of the 2-methyl group in the membrane
412 compared to 2Me-Dip (Rog et al., 2007 ; Poger & Mark, 2013), which may
413 explain the difference between 2Me-BHT and 2Me-Dip in rigidifying membranes
414 with different compositions. Future research will illuminate whether there are
415 additional interactions between hopanoids and other membrane constituents (*e.g.*
416 proteins or cell wall components) that facilitate survival under stress.

417 Finally, it is important to keep in mind that (2Me)-hopanoids may act
418 locally rather than globally with respect to influencing membrane biophysical
419 properties. In our *in vitro* experiments, we did not observe a significant difference
420 in membrane rigidity when less than 10 mol% of (2Me)-hopanoids were used
421 (Figure 6). This may be due to a critical concentration needed to trigger an effect,
422 which is consistent with molecular dynamic simulations that demonstrate
423 cholesterol starts to self-organize within membranes at concentration above 10
424 mol% (Martinez-Seara et al., 2010). However, we hasten to point out that the
425 mol% of (2Me)-hopanoids in the native membrane experiment (Figure 8) are not

426 directly comparable to those using model lipids (Figure 6) due to the presence of
427 endogenous hopanoids in *ΔhpnP* membranes. The existence of BHT in Δ*hpnP*
428 may explain why the membrane rigidifying effect of exogenously-added BHT is
429 saturated at 10 mol% in the *E. coli* PLE but has no impact on *R. palustris* TIE-1
430 IM and OM. In this context, it is noteworthy that cardiolipin significantly increases
431 in the absence of all hopanoids (Neubauer et al., 2014). In *E. coli*, cardiolipin
432 localizes to negatively curved regions of the cell (Renner & Weibel, 2011).
433 Looking beyond the function of methylation, it is possible that certain hopanoid
434 types could fulfill the geometry requirements of curved membranes and facilitate
435 cell division or vesicle formation, consistent with both the microdomain features
436 observed in prior subcellular hopanoid localization studies (Doughty et al., 2014)
437 and the strong cell division defect displayed by a mutant lacking the ability to
438 transport hopanoids to the OM (Doughty et al., 2014). Going forward,
439 consideration of other roles for structurally diverse hopanoids, including the
440 possibility that some might influence membrane protein function (Phillips et al.,
441 2009), modify specific proteins or cell wall components through covalent linkages
442 (Jeong & McMahon, 2002 ; Silipo et al., 2014), or even play a role in signaling
443 pathways in analogy to cholesterol and phosphatidylcholine (Kuwabara &
444 Labouesse, 2002 ; Aktas et al., 2010), will enhance our appreciation for this
445 ancient lipid class.

446

447 **Materials and Methods**

448 **Bacterial strains and chemicals.**

449 *Rhodopseudomonas palustris* TIE-1 wild type (WT) and mutant strains were
450 grown as previously described (Welander et al., 2012). Purified hopanoids
451 ((2Me)-diplopterol, (2Me)-bacteriohopanetetrol (BHT)) were obtained by following
452 the purification protocols (Wu et al., 2014). *E. coli* polar lipid extract and 1,2-
453 dioleoyl-*sn*-glycero-3-phosphocholine (DOPC), 1,2-diheptadecanoyl-*sn*-glycero-
454 3-phosphocholine (PC(17:0/17:0)), 1,2-diheptadecanoyl-*sn*-glycero-3-
455 phosphoethanolamine (PE(17:0/17:0)), 1,2-diheptadecanoyl-*sn*-glycero-3-
456 phospho-(1'-*rac*-glycerol) (PG(17:0/17:0)) were from Avanti Polar Lipids.
457 Squalene, cholesterol, pyridine, acetic anhydride, morpholinepropanesulfic acid
458 (MOPS), 4-(2-hydroxyethyl)-1-piperazineethanesulfonic acid (HEPES), sodium
459 succinate, 1,6-diphenyl-1,3,5-hexatriene (DPH), Percoll, and tetrahydrofuran
460 (THF) were from Sigma-Aldrich. Yeast extract was from HIMEDIA. Peptone was
461 from BD Biosciences. Methanol and dichloromethane (DCM) were HPLC grade
462 from Alfa Aesar.

463 **Whole cell membrane fluidity measurements.**

464 To prepare bacterial cells for measurements of membrane fluidity, single colonies
465 of *R. palustris* TIE-1 WT and mutants were inoculated into 10 mL YPMS (0.3%
466 yeast extract, 0.3% peptone, 50 mM MOPS, 5 mM succinate, pH 7.0) and grown
467 at 30 °C, 250 rpm for ~72 hr to reach late stationary phase (OD_{600} ~1.0). The
468 cells (250 μL) were spun down and the cell pellets were washed once with 50

mM HEPES, 50 mM NaCl, pH 7.0 (buffer A). Pellets were resuspended in different amounts of the same buffer to adjust the final OD_{600} to ~0.2. To measure membrane fluidity, 4.3 μL of DPH (736 μM stock solution in ethanol; the concentration was determined by ε350nm = 88 $cm^{-1}mM^{-1}$ in methanol) was added into 400 μL of the cell suspension. Samples were incubated in a 25 °C or 40 °C water bath without light for 30 min, followed by measurements of fluorescence polarization (Fluorolog, HORIBA Instruments. Instrument parameter: ex 358 nm, slit = 3 mm; em 428 nm, slit = 7 mm; integration time = 1 sec) (Lin et al., 2011). Three biological replicates were measured, each containing 6-14 technical replicates. To reduce bias from the stability of the instrument and the samples, especially at 40 °C, we randomized our data acquisition sequence. *P* value in this manuscript represents t-test using two-tailed equal variance.

Membrane fractionation using Percoll gradient.

To prepare cell cultures for membrane fractionation, single colonies of *R. palustris* TIE-1 WT or Δ*hpnP* mutant were inoculated into 10 mL YPMS and grown for ~4 days at 30 °C, 250 rpm. The culture (0.5 mL) was then inoculated into 1 L of YPMS in a 2 L flask and grown at 30 °C, 250 rpm for 4 days before harvesting by centrifugation at 12,000 g for 20 min at RT. The typical yield was ~1.8 g of wet cell paste per 1 L culture. To estimate the yield in dried cells, a

490 small aliquot of the wet cell paste was lyophilized until there was no further
491 change in weight. On average the weight of dried cells was one third of wet cells.
492 The wet cell pastes were stored at -80 °C before cell lysis.

493 To lyse the cells, 19 mL of buffer A was added into ~3.6 g of cells (from 2
494 L culture) and passed through a French Press twice at 14,000 psi, followed by
495 sonication (Sonic Dismembrator 550, Fisher Scientific, 1/8 inch tip, power output
496 3.5, 1 sec on, 4 sec off, total on time 5 min at 4 °C). The cell debris was spun
497 down at 20,000 g, 20 min at 4 °C. The supernatant containing cell membranes
498 was transferred into 4 mL ultracentrifugation tubes (~3 mL sample per tube) and
499 centrifuged at 80,000 rpm in a TLA-100.3 rotor for 1 hr at 4 °C (Optima MAX
500 Ultracentrifuge, Beckman Coulter). The resulting membrane pellets in each tube
501 were resuspended in 300 μL buffer A by pipetting while being sonicated in a bath
502 sonicator (VWR B2500A-DTH, 42 kHz, RF Power 85 W). The suspension was
503 combined into one single tube and sonicated again using the probe sonicator
504 (power level 2.5, 1 sec on, 4 sec off, total on time 2.5 min, 4 °C).

505 To separate inner and outer membranes, ~320 μL of membrane samples
506 were laid on top of 3 mL 18% Percoll (v/v in buffer A), followed by
507 ultracentrifugation at 30,000 rpm in a TLA 100.3 rotor at 4 °C for 15 min (Morein
508 et al., 1994). Three visually distinct bands were formed and a pipetman was used
509 to take in sequence of the top band (1 mL), bottom band (~200-250 μL) and the
510 middle band (0.7-1 mL) (Figure 3). The top and bottom bands constituted the IM

511 and OM, determined by the presence and absence of NADH-oxidase activity,
512 respectively. The band on top of the OM was less defined and exhibited some
513 NADH-oxidase activity, which may be an artifact from sonication steps that mixed
514 the IM and OM, and we therefore discarded it in our subsequent studies. To
515 remove Percoll, samples from the same band were combined and centrifuged in
516 a TLA 100.3 rotor at 50,000 rpm at 4 °C for 1.5 hr. After centrifugation, a layer of
517 the fractionated membrane was formed on top of a transparent Percoll layer
518 (Figure 3). The membrane layers were collected by pipetting gently in water
519 and/or scraped gently using a metal spatula. The membrane samples were then
520 frozen at -20 °C before being lyophilized. The total lipid extractions (TLE) from
521 the lyophilized membranes were obtained by modified Bligh-Dyer extraction
522 according to published protocols (Kulkarni et al., 2013).

523

524 **Quantification of lipid compositions of inner and outer membranes of *R.***
525 ***palustris* TIE-1.**

526 GC-MS (Thermo Scientific Trace-GC/ISQ mass spectrometer with a Restek Rxi-
527 XLB column (30 m × 0.25 mm × 0.10 μm)) was used to quantify hopanoids from
528 the TLE from the IM and OM. An internal standard, androsterone (750 ng) was
529 air dried with 100 μg of the TLE overnight at RT and derivatized with 50 μL acetic
530 anhydride and 50 μL pyridine at 60 °C for 30 min, followed by GC-MS analyses
531 as described (Welander et al., 2009 ; Kulkarni et al., 2013). To account for the

532 difference in ionization efficiencies between androsterone and hopanoids,
533 calibration curves using androsterone and purified hopanoids were generated to
534 quantify hopanoids (Wu et al., 2014).

535 LC-MS (Waters Acquity UPLC/Xevo G2-S time-of-flight mass
536 spectrometer with a CSH C18 column (2.1 x 100 mm x 1.7 μm)) was used to
537 quantify both phospholipids and hopanoids. Phospholipid internal standards
538 (PC(17:0/17:0), PE(17:0/17:0), PG(17:0/17:0), 1 μg each) were mixed with 100
539 μg of the TLE from fractionated membranes and air-dried overnight at RT. LC
540 solvent (200 μL, Isopropanol:acetonitrile:water = 2:1:1) was then added into the
541 samples, followed by sonication before analyses by LC-MS as described earlier
542 (Malott et al., 2014 ; Wu et al., 2014). The column temperature was maintained
543 at 55 °C. A binary solvent system containing solvent A (acetonitrile:water; 60:40)
544 and solvent B (isopropanol:acetonitrile; 90:10), both with 10 mM ammonium
545 formate and 0.1% formic acid was used. The flow rate was set at 400 μL/min and
546 the elution program started at 40% B, increased linearly to 43% B in 2 min, then
547 to 50% B in 0.1 min, followed by a linear increase to 54% B over 9.9 min, a jump
548 to 70% B in 0.1 min, another linear increase to 99% B over 5.9 min, a
549 subsequent decrease to 40% B in 0.1 min, and then maintained at the same level
550 for 1.9 min.

551 The eluents from the column were ionized by electrospray ionization (ESI).
552 MS^E data from 100 to 1500 m/z was collected in either the positive or negative

ion mode. MS^E consists of both low energy and high energy scans were obtained simultaneously. During data analysis product ions can be associated with parent ions if they are coincident in chromatographic time. Electrospray conditions were capillary voltage 2.0 kV, cone voltage 30 V, source offset 60 V, source temperature 120 °C, desolvation temperature 550 °C, cone gas 20 L/h, and desolvation gas 900 L/h. The TOF-MS was run in resolution mode, typically 32,000 m/Δm. The mass axis was calibrated with sodium formate clusters. Leucine enkephalin was used as a mass reference during acquisition. The data were collected in continuum mode, and then converted to centroid mode for quantitative analysis using the Quanlynx program (Waters Corporation, Milford, MA) (Wu et al., 2014).

Membrane fluidity measurements in small unilamellar vesicles (SUVs).

Cholesterol, squalene, and hopanoid stock solutions were prepared at 1 mg/mL in THF and the *E. coli* PLE and DOPC were prepared at 10 mg/mL in DCM. To prepare lipid mixture, a total of 1 μmol of lipid was added into 0.5 mL of DCM and dried in a rotary evaporator. Because any residual solvents can cause high errors in fluidity measurements, the samples were placed under vacuum overnight to ensure complete removal of organic solvents.

573 To prepare SUVs, 1 mL of buffer A was added into the glass vials
574 containing dried lipid mixtures. Samples were suspended by sonication for 1 hr at
575 RT in a bath sonicator (VWR B2500A-DTH, 42 kHz, RF Power 85 W). The
576 suspended lipids (murky giant multilamellar vesicles) were transferred into 1.5
577 mL eppendorf and flash frozen in liquid nitrogen for 3 min, followed by thawing in
578 a 37 °C water bath for 3 min. This freeze-thaw cycle, which breaks down the
579 giant vesicles into smaller ones, was repeated two more times. SUVs were
580 prepared by passing the samples through 0.1 μm polycarbonate membranes
581 (Whatman) using Avanti mini-Extruder at RT (Avanti Polar Lipids). The extrusion
582 was performed a total of 11 times and the vesicle suspension became clear
583 during the process. The sizes and stability of the SUVs was determined by
584 dynamic light scattering (Wyatt DynaPro NanoStar. Instrument parameters:
585 acquisition time 5 sec, number of acquisition 10, laser wavelength 659 nm, laser
586 power 10%, 25 °C). The average size distribution of the SUVs was between 80 to
587 90 nm and remained stable for at least 4 hr at RT.

588 SUVs after extrusion were diluted 1:1 in buffer A to reach a final
589 concentration of 0.5 mM (400 μL total volume). DPH (1.8 μL of 44.5 μM stock
590 solution in ethanol) was added into the sample and vortexed immediately. The
591 SUV-DPH samples were incubated in 25 °C or 40 °C water bath without light for
592 at least 30 min before the fluorescence polarization was measured using the
593 parameters described above. The concentration of the fluorescence reporter dye

DPH and the instrument parameters were optimized to have a strong and linear signal output.

Membrane fluidity measurements using total lipid extract from inner and outer membranes of *R. palustris* TIE-1.

Different amounts of purified hopanoids (5, 10, and 20 nmol) were added to 100 nmol of the inner or outer membrane extracts of Δ*hpnP* (assuming average molecular weight is 786 g/mol). The same procedures as described above were followed for the preparation of SUVs. Buffer A (600 μL) was used to suspend the dried lipids so that the final lipid concentrations before the addition of DPH were between 0.088 and 0.1 mM (400 μL sample volume). To measure fluorescence polarization, DPH (1.8 μL of 7.4 μM stock solution in ethanol) was used (the final concentration of DPH was 0.03 μM, which was ~0.03 mol% of the total lipids in the sample). Controls of membranes from WT or Δ*hpnP* only without addition of hopanoids were included.

Acknowledgements

We thank the members of the Newman lab for critical comments on the manuscript. We thank Dr. Nathan Dalleska for help with UPLC-TOF-MS. The UPLC-TOF-MS equipment in the California Institute of Technology's Environmental Analysis Center was used in the work. We thank Dr. Heun Jin Lee

and Dr. Eva Schmid for vesicle preparation advice. This work was supported by grants from NASA (NNX12AD93G), the National Science Foundation (1224158), and the Howard Hughes Medical Institute (HHMI) to DKN. DKN is an HHMI Investigator.

References

Aktas M, Wessel M, Hacker S, Klusener S, Gleichenhagen J, Narberhaus F (2010) Phosphatidylcholine biosynthesis and its significance in bacteria interacting with eukaryotic cells. *Eur J Cell Biol,* **89**, 888-894.

Bloch KE (1979) Speculations on the Evolution of Sterol Structure and Function. *Crc Cr Rev Bioch Mol,* **7**, 1-5.

Brocks JJ, Love GD, Summons RE, Knoll AH, Logan GA, Bowden SA (2005) Biomarker evidence for green and purple sulphur bacteria in a stratified Palaeoproterozoic sea. *Nature,* **437**, 866-870.

Brocks JJ, Pearson A (2005) Building the biomarker tree of life. *Rev Mineral Geochem,* **59**, 233-258.

Brugger B, Erben G, Sandhoff R, Wieland FT, Lehmann WD (1997) Quantitative analysis of biological membrane lipids at the low picomole level by nano-electrospray ionization tandem mass spectrometry. *P Natl Acad Sci USA,* **94**, 2339-2344.

635 Doughty DM, Hunter R, Summons RE, Newman DK (2009) 2-Methylhopanoids
636 are maximally produced in akinetes of *Nostoc punctiforme*: geobiological
637 implications. Geobiology, **7**, 524–532.
638 Doughty DM, Coleman ML, Hunter RC, Sessions AL, Summons RE, Newman
639 DK (2011) The RND-family transporter, HpnN, is required for hopanoid
640 localization to the outer membrane of *Rhodopseudomonas palustris* TIE-1.
641 *P Natl Acad Sci USA,* **108**, E1045-E1051.
642 Doughty DM, Dieterle M, Sessions AL, Fischer WW, Newman DK (2014) Probing
643 the subcellular localization of hopanoid lipids in bacteria using NanoSIMS.
644 *Plos One,* **9**, e84455.
645 Furey A, Moriarty M, Bane V, Kinsella B, Lehane M (2013) Ion suppression; A
646 critical review on causes, evaluation, prevention and applications. *Talanta,*
647 **115**, 104-122.
648 Gallet A (2011) Hedgehog morphogen: from secretion to reception. *Trends Cell*
649 *Biol,* **21**, 238-246.
650 Gibson KE, Kobayashi H, Walker GC (2008), Molecular determinants of a
651 symbiotic chronic infection, *Annu Rev Genet*, **42,** 413-441.
652 Hanukoglu I (1992) Steroidogenic enzymes - structure, function, and role in
653 regulation of steroid-hormone biosynthesis. *J Steroid Biochem,* **43**, 779-
654 804.
655 Hope MJ, Bally MB, Webb G, Cullis PR (1985) Production of large unilamellar
656 vesicles by a rapid extrusion procedure: characterization of size

distribution, trapped volume and ability to maintain a membrane potential. *Biochim Biophys Acta,* **812**, 55-65.

Jeong J, Mcmahon AP (2002) Cholesterol modification of Hedgehog family proteins. *J Clin Invest,* **110**, 591-596.

Kannenberg E, Blume A, Geckeler K, Poralla K (1985) Properties of Hopanoids and Phosphatidylcholines Containing Omega-Cyclohexane Fatty-Acid in Monolayer and Liposome Experiments. *Biochim Biophys Acta,* **814**, 179-185.

Kannenberg E, Blume A, Mcelhaney RN, Poralla K (1983) Monolayer and calorimetric studies of phosphatidylcholines containing branched-chain fatty-acids and of their iteractions with cholesterol and with a bacterial hopanoid in model membranes. *Biochim Biophys Acta,* **733**, 111-116.

Knoll AH, Summons RE, Waldbauer JR, Zumberge JE (2007) The geological succession of primary producers in the oceans. In: *In The Evolution of Primary Producers in the Sea* (eds Falkowski P, Knoll AH). Academic Press, Boston, pp. 133-164.

Kulkarni G, Wu CH, Newman DK (2013) The general stress response factor EcfG regulates expression of the C-2 hopanoid methylase HpnP in *Rhodopseudomonas palustris* TIE-1. *J Bacteriol,* **195**, 2490-2498.

Kuwabara PE, Labouesse M (2002) The sterol-sensing domain: multiple families, a unique role? *Trends Genet,* **18**, 193-201.

678 Lin ZF, Liu N, Lin GZ, Peng CL (2011) Factors altering the membrane fluidity of
679 spinach thylakoid as determined by fluorescence polarization. *Acta*
680 *Physiol Plant,* **33**, 1019-1024.
681 Lipowsky R, Sackmann E (1995) *Structure and Dynamics of Membranes I. From*
682 *Cells to Vesicles / II. Generic and Specific Interactions,* Elsevier.
683 Los DA, Murata N (2004) Membrane fluidity and its roles in the perception of
684 environmental signals. *Bba-Biomembranes,* **1666**, 142-157.
685 Malott RJ, Steen-Kinnaird BR, Lee TD, Speert DP (2012) Identification of
686 Hopanoid Biosynthesis Genes Involved in Polymyxin Resistance in
687 *Burkholderia multivorans*. *Antimicrob Agents Ch,* **56**, 464-471.
688 Malott RJ, Wu C-H, Lee TD, Hird TJ, Dalleska NF, Zlosnik JE, Newman DK,
689 Speert DP (2014) Fosmidomycin decreases membrane hopanoids and
690 potentiates the effects of colistin on *Burkholderia multivorans* clinical
691 isolates. *Antimicrob Agents Ch,* **58**, 5211-5219.
692 Martinez-Seara H, Rog T, Karttunen M, Vattulainen I, Reigada R (2010)
693 Cholesterol induces specific spatial and orientational order in
694 cholesterol/phospholipid membranes. *Plos One,* **5**.
695 Matsumoto K, Kusaka J, Nishibori A, Hara H (2006) Lipid domains in bacterial
696 membranes. *Mol Microbiol,* **61**, 1110-1117.
697 Miao L, Nielsen M, Thewalt J, Ipsen JH, Bloom M, Zuckermann MJ, Mouritsen
698 OG (2002) From lanosterol to cholesterol: Structural evolution and
699 differential effects on lipid bilayers. *Biophys J,* **82**, 1429-1444.

700 Morein S, Henricson D, Rilfors L (1994) Separation of inner and outer-membrane
701 vesicles from *Escherichia coli* in self-generating percoll gradients. *Anal*
702 *Biochem,* **216**, 47-51.
703 Myers DS, Ivanova PT, Milne SB, Brown HA (2011) Quantitative analysis of
704 glycerophospholipids by LC-MS: Acquisition, data handling, and
705 interpretation. *Bba-Mol Cell Biol L,* **1811**, 748-757.
706 Nagumo A, Sato Y, Suzuki Y (1991) Electron-spin-resonance studies of
707 phosphatidylcholine interacted with cholesterol and with a hopanoid in
708 liposomal membrane. *Chem Pharm Bull,* **39**, 3071-3074.
709 Neidhardt FC, Curtiss R (1996) *Escherichia coli and Salmonella : Cellular and*
710 *Molecular Biology,* ASM Press, Washington, D.C.
711 Neubauer C, Dalleska NF, Cowley ES, Shikuma NJ, Wu C-H, Sessions AL,
712 Newman DK (2014) Lipid remodeling in *Rhodopseudomonas palustris*
713 TIE-1 upon loss of hopanoids and hopanoid methylation. *submitted*.
714 Ourisson G, Albrecht P, Rohmer M (1984) The Microbial Origin of Fossil-Fuels.
715 *Sci Am,* **251**, 44-&.
716 Ourisson G, Rohmer M (1992) Hopanoids .2. Biohopanoids - a novel class of
717 bacterial lipids. *Accounts Chem Res,* **25**, 403-408.
718 Ourisson G, Rohmer M, Poralla K (1987) Prokaryotic Hopanoids and Other
719 Polyterpenoid Sterol Surrogates. *Annu Rev Microbiol,* **41**, 301-333.
720 Pearson A (2013) *Lipidomics for Geochemistry,* Elsevier, London.

721 Phillips R, Ursell T, Wiggins P, Sens P (2009) Emerging roles for lipids in
722 shaping membrane-protein function. *Nature,* **459**, 379-385.
723 Poger D, Mark AE (2013) The relative effect of sterols and hopanoids on lipid
724 bilayers: when comparable is not identical. *J Phys Chem B,* **117**, 16129-
725 16140.
726 Poralla K, Kannenberg E, Blume A (1980) A glycolipid containing hopane
727 isolated from the acidophilic, thermophilic *Bacillus acidocaldarius*, has a
728 cholesterol-like function in membranes. *FEBS letters,* **113**, 107-110.
729 Rasmussen B, Fletcher IR, Brocks JJ, Kilburn MR (2008) Reassessing the first
730 appearance of eukaryotes and cyanobacteria. *Nature,* **455**, 1101-1104.
731 Renner LD, Weibel DB (2011) Cardiolipin microdomains localize to negatively
732 curved regions of *Escherichia coli* membranes. *P Natl Acad Sci USA,* **108**,
733 6264-6269.
734 Ricci JN, Coleman ML, Welander PV, Sessions AL, Summons RE, Spear JR,
735 Newman DK (2014) Diverse capacity for 2-methylhopanoid production
736 correlates with a specific ecological niche. *ISME J,* **8**, 675-684.
737 Ricci JN, Michel A, Newman DK (2015) Phylogenetic analysis of *hpnP* reveals
738 the origin of 2-methylhopanoid production in Alphaproteobacteria.
739 *Geobiology*, *in press*.
740 Rog T, Pasenkiewicz-Gierula M, Vattulainen I, Karttunen M (2007) What
741 happens if cholesterol is made smoother: Importance of methyl

substituents in cholesterol ring structure on phosphatidylcholine-sterol interaction. *Biophys J,* **92**, 3346-3357.

Rohmer M, Bouvier P, Ourisson G (1979) Molecular evolution of biomembranes: structural equivalents and phylogenetic precursors of sterols. *Proc Natl Acad Sci U S A,* **76**, 847-851.

Sáenz JP (2010) Hopanoid enrichment in a detergent resistant membrane fraction of *Crocosphaera watsonii*: Implications for bacterial lipid raft formation. *Org Geochem,* **41**, 853-856.

Sáenz JP, Sezgin E, Schwille P, Simons K (2012) Functional convergence of hopanoids and sterols in membrane ordering. *Proc Natl Acad Sci U S A,* **109**, 14236-14240.

Schmerk CL, Bernards MA, Valvano MA (2011) Hopanoid Production Is Required for Low-pH Tolerance, Antimicrobial Resistance, and Motility in *Burkholderia cenocepacia*. *J Bacteriol,* **193**, 6712-6723.

Silipo A, Vitiello G, Gully D, Sturiale L, Chaintreuil C, Fardoux J, Gargani D, Lee H-I, Kulkarni G, Busset N, Marchetti R, Palmigiano A, Moll H, Engel R, Lanzetta R, Paduano L, Parrilli M, Chang W-S, Holst O, Newman DK, Garozzo D, D'errico G, Giraud E, Molinaro A (2014) Hopanoid-Lipid A, a new component improving bacterial membrane resistance. *Nat Comm*, *in press*.

Song YL, Kenworthy AK, Sanders CR (2014) Cholesterol as a co-solvent and a ligand for membrane proteins. *Protein Sci,* **23**, 1-22.

764 Summons RE, Jahnke LL, Hope JM, Logan GA (1999) 2-Methylhopanoids as
765 biomarkers for cyanobacterial oxygenic photosynthesis. *Nature,* **400**, 554-
766 557.
767 Summons RE, Walter MR (1990) Molecular Fossils and Microfossils of
768 Prokaryotes and Protists from Proterozoic Sediments. *Am J Sci,* **290A**,
769 212-244.
770 Vanblitterswijk WJ, Vandermeer BW, Hilkmann H (1987) Quantitative
771 contributions of cholesterol and the individual classes of phospholipids
772 and their degree of fatty acyl (un)saturation to membrane fluidity
773 measured by fluorescence polarization. *Biochemistry-Us,* **26**, 1746-1756.
774 Welander PV, Coleman ML, Sessions AL, Summons RE, Newman DK (2010)
775 Identification of a methylase required for 2-methylhopanoid production and
776 implications for the interpretation of sedimentary hopanes. *Proc Natl Acad*
777 *Sci U S A,* **107**, 8537-8542.
778 Welander PV, Doughty DM, Wu CH, Mehay S, Summons RE, Newman DK
779 (2012) Identification and characterization of *Rhodopseudomonas palustris*
780 TIE-1 hopanoid biosynthesis mutants. *Geobiology,* **10**, 163-177.
781 Welander PV, Hunter RC, Zhang LC, Sessions AL, Summons RE, Newman DK
782 (2009) Hopanoids play a role in membrane integrity and pH homeostasis
783 in *Rhodopseudomonas palustris* TIE-1. *J Bacteriol,* **191**, 6145-6156.

784 Wu C-H, Kong L, Bialecka-Fornal M, Park S, Thompson AL, Kulkarni G, Conway
785 SJ, Newman DK (2014) Purification and synthesis of hopanoids as
786 standards for mass spectrometry. *submitted*.

787

788

789 Table 1: Mutant strains used for the whole cell membrane rigidity measurements.

790 The function of the gene and the effect of its deletion are listed.

Gene	Function	Deletion effect
shc (hpnF)	Cyclization of squalene to form C30 hopanoids (diploptene and diplopterol)	No hopanoid production and accumulation of squalene
hpnH	Addition of adenosine to diploptene to generate adenosylhopane, a precursor for extended hopanoid production	No extended hopanoid production, accumulation of C30 hopanoids
hpnG	Removal of adenine from adenosyl hopane	No BHT and aminoBHT production, accumulation of adenosylhopane
hpnN	An IM transporter that transports hopanoids to the outer membrane	Absence of hopanoids in the OM and accumulation of hopanoids in the IM
hpnO	Production of aminoBHT	No aminoBHT production
hpnP	Methyl transfer to A ring at C-2	No hopanoid methylation

791

792 Table 2: Purification yields of membrane fractionation using Percoll gradient. The
793 yields in weight% of membrane fractionation Errors represent standard deviation
794 from three biological replicates.

795

		Weight % membranes in dry cells	total	Weight % TLE in membranes
WT	inner	4.7 ± 0.5		12.4 ± 0.8
	mix	3.7 ± 1.2		5.6 ± 0.1
	outer	3.3 ± 0.4	11.6 ± 1.4	4.9 ± 0.6
Δ*hpnP*	inner	4.2 ± 1.3		15 ± 2.3
	mix	2.3 ± 0.8		8.3 ± 2.3
	outer	2.9 ± 0.6	9.4 ± 2.2	5.3 ± 1.4

796

797

798

799

800 Table 3: Annotation of phospholipids identified by LC-MS analyses (see Figure 7).
801 The types of lipids (PC: phosphatidylcholine, PE: phosphotidylethanolamine, PG:
802 phosphatidylglycerol, CL: cardiolipin, cyc: cyclopropanation; the first number
803 indicates the total number of carbon of the fatty acid chains and the second
804 number indicates the number of double bonds in these chains) and their retention
805 time (min) and m/z value of the base peak are shown. For PC and PE, the base
806 peak is the proton adduct and for CL, the base peak is the mmonium adduct. For
807 PG, the base peak indicates a loss of glycerophosphate (-171 m/z).

808

Compound	**RT (min)**	**$[M+H]^+$**	**$[M-C_3H_7O_2HPO_4]^+$**	**$[M+NH_4]^+$**
PG32:1	4.39		549.4895	
PG34:2	4.89		575.505	
PC34:2	5.94	758.5694		
PG34:1	6.11		577.5208	
PG36:2	6.2		603.5364	
PE34:2	6.38	716.5225		
PC_cyc35:1	6.76	772.5851		
PG_cyc35	6.95		591.5364	
PG_cyc37:1	7.05		617.5521	
PC(35:2)	7.06	772.5851		
PE_cyc35:1	7.28	730.5381		
PC34:1	7.51	760.5851		
PC36:2	7.65	786.6007		
PG(17:0/17:0)	7.86		579.5364	
PG36:1	7.99		605.5521	
PE34:1	8.14	718.5381		
PE36:2	8.27	744.5538		
PC_cyc35	8.58	774.6007		
PC_cyc37:1	8.72	800.6164		
PE_cyc35	9.28	732.5538		
PE_cyc37:1	9.42	758.5694		
PC(17:0/17:0)	9.75	762.6007		
PC36:1	9.91	788.6164		
PE(17:0/17:0)	10.53	720.5538		
PE36:1	10.71	746.5694		
PC_cyc37	11.23	802.632		
PE_cyc37	12.1	760.5851		
PC36:0	12.79	790.634		
PE36	12.98	748.5851		
PC36:4	13.39	782.569		
CL70:4	15.09			1447.0373
CL68:3	15.1			1421.0217
CL72:4	15.31			1475.0686

CL70:3	15.34			1449.053
CL68:2	15.35			1423.0373
CL72:3	15.58			1477.0843
CL70:2	15.6			1451.0686

811

812 Table 4: Phospholipid compositions in the inner membrane (IM) and outer
813 membrane (OM) of *R. palustris* TIE-1 WT and Δ*hpnP* analyzed by LC-MS.

		Weight % of TLE			
Compound	RT	WT IM	WT OM	Δ*hpnP* IM	Δ*hpnP* OM
PC36:2	7.65	5.15 ± 0.47	5.34 ± 0.26	5.44 ± 0.57	5.94 ± 0.48
PC_cyc37:1	8.72	4.33 ± 0.45	4.01 ± 0.48	4.07 ± 1.13	3.96 ± 1.24
PC36:1	9.91	2.90 ±0.3	1.84 ± 0.52	2.59 ± 0.93	2.15 ± 1.08
PC34:1	7.51	2.66 ± 0.22	2.23 ± 0.33	2.53 ± 0.58	2.38 ± 0.57
PC34:2	5.94	1.56 ± 0.12	1.24 ± 0.44	1.41 ± 0.51	1.44 ± 0.48
PC_cyc35	8.58	0.23 ± 0.01	0.14 ± 0.05	0.20 ± 0.07	0.17 ± 0.1
PC_cyc35:1	6.76	0.12 ± 0.01	0.07 ± 0.02	0.11 ± 0.04	0.09 ± 0.06
PC(35:2)	7.06	0.09 ± 0.01	0.05 ± 0.03	0.08 ± 0.03	0.06 ± 0.05
PC_cyc37	11.23	0.07 ± 0.01	0.04 ± 0.01	0.06 ± 0.02	0.05 ± 0.03
PC36:0	12.79	0.02 ± 0	0.01 ± 0	0.02 ± 0.01	0.01 ± 0.01
	Sum	**17.12**	**14.96**	**16.50**	**16.25**
PE_cyc37:1	9.42	4.92 ± 0.36	3.36 ± 0.94	4.68 ± 1.5	4.18 ± 1.64
PE34:1	8.14	2.49 ± 0.19	1.44 ± 0.49	2.28 ± 0.84	1.82 ± 0.92
PE36:1	10.71	2.29 ± 0.28	1.08 ± 0.38	2.05 ± 0.85	1.43 ± 0.95
PE36:2	8.27	1.88 ± 0.21	1.22 ± 0.46	1.74 ± 0.65	1.59 ± 0.72
PE34:2	6.38	0.43 ± 0.02	0.23 ± 0.08	0.42 ± 0.16	0.33 ± 0.21
PE_cyc35	9.28	0.20 ± 0.02	0.11 ± 0.04	0.19 ± 0.07	0.15 ± 0.09
PE_cyc35:1	7.28	0.12 ± 0.01	0.06 ± 0.02	0.11 ± 0.05	0.09 ± 0.06
PE_cyc37	12.1	0.07 ± 0.01	0.04 ± 0.01	0.07 ± 0.02	0.05 ± 0.03
PE36	12.98	0.04 ± 0	0.03 ± 0.01	0.04 ± 0.01	0.03 ± 0.01
	Sum	**12.44**	**7.58**	**11.58**	**9.67**
PG36:2	6.2	2.59 ± 0.24	1.68 ± 0.54	2.25 ± 0.67	1.87 ± 0.8
PG36:1	7.99	1.13 ± 0.08	0.69 ± 0.19	0.98 ± 0.31	0.81 ± 0.35
PG34:1	6.11	0.77 ± 0.17	0.5 ± 0.2	0.6 ± 0.24	0.51 ± 0.19
PG_cyc37:1	7.05	0.11 ± 0.02	0.07 ± 0.05	0.08 ± 0.02	0.07 ± 0.04
PG34:2	4.89	0.05 ± 0	0.03 ± 0.01	0.04 ± 0.01	0.03 ± 0.02
PG_cyc35	6.95	0.02 ± 0	0.01 ± 0	0.02 ± 0.01	0.01 ± 0.01
PG32:1	4.39	0.00 ± 0	0.01 ± 0	0 ± 0	0.01 ± 0
	Sum	**4.67**	**3**	**3.97**	**3.31**
PC+PE+PG	**Total % of TLE**	**34.23**	**25.54**	**32.06**	**29.23**

814

815

Figure Legends

Figure 1. Structures of selected hopanoids, cholesterol and squalene.

Figure 2. Whole cell membrane fluidity. Error bars represent the standard deviation from three biological replicates (total 21-26 technical replicates).

Figure 3. Membrane fractionation and hopanoids analysis using GC-MS. (A) Three distinct bands were formed after ultracentrifugation in a Percoll gradient. (B) The bands were recovered and resuspended. (C) Samples were ultracentrifuged to pellet down the purified membranes, which sat on top of a transparent solid Percoll layer. (D) GC-MS of fractionated membranes of *R. palustris* TIE-1 WT and Δ*hpnP*.

Figure 4. Molar percentage of hopanoids in the inner membrane (IM) and outer membrane (OM) of WT and Δ*hpnP* determined by GC-MS. Error bars represent the standard deviation from three biological replicates. Total hopanoids = sum of (2Me)-Dip and (2Me)-BHT.

Figure 5. Partitioning of hopanoids in the inner membrane (IM) and outer mebraane (OM) of *R. palustris* TIE-1. (A) Molar ratio between short (Dip and 2Me-Dip) and long (BHT and 2Me-BHT) hopanoids in WT and Δ*hpnP*. (B) Molar ratio between methylated and desmethylated hopanoid in WT. Error bars represent the standard deviation from three biological replicates. **P* = 0.015; ***P* < 0.01.

Figure 6. Membrane rigidity measurements at 25 °C using model lipids. (A) dioleoyl phosphatidylcholine (DOPC) and (B) *E. coli* polar lipid extract (PLE) were mixed with different mol% of cholesterol, squalene, and hopanoids. Error bars represent the standard deviation from three biological replicates (total 21 technical replicates).

Figure 6-figure supplement 1. Membrane rigidity measurements at 25 °C and 40 °C using model lipids. (A) DOPC and (B) *E. coli* polar lipid extract (PLE) were mixed with different mol% of cholesterol, squalene, and hopanoids. Error bars represent standard deviation from three biological replicates (total 21 technical replicates).

Figure 7. LC-MS profiles of the inner membrane (IM) and outer membrane (OM) of *R. palustris* TIE-1 WT and Δ*hpnP*.

Figure 8. Membrane rigidity measurements at 25 °C using total lipid extract from *R. palustris* TIE-1 inner membrane (IM) and outer membrane (OM). The IM (A) or OM (B) from Δ*hpnP* were mixed with different mol% of hopanoids. Error bars represent the standard deviation from three biological replicates (total 21 technical replicates). **P* < 0.001 (relative to Δ*hpnP*).

Figure 8-figure supplement 1. Membrane rigidity measurements at 40 °C using total lipid extract from *R. palustris* TIE-1 inner membrane (IM) and outer membrane (OM). The IM (A) or OM (B) from Δ*hpnP* were mixed with different

856 mol% of hopanoids. Small unilamellar vesicles from the lipid mixtures were
857 prepared and the membrane rigidity was measured by fluorescence polarization
858 of a reporter dye diphenyl hexatriene. Error bars represent standard deviation
859 from three biological replicates (total 21 technical replicates).

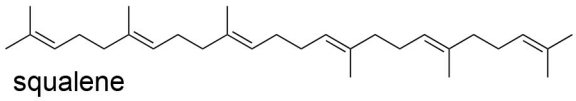

squalene

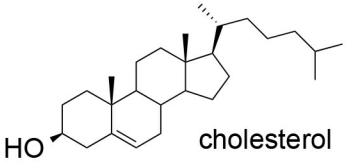

cholesterol

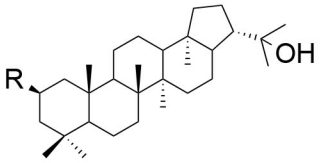

diplopterol (Dip) R = H

2Me-diplopterol R = CH_3

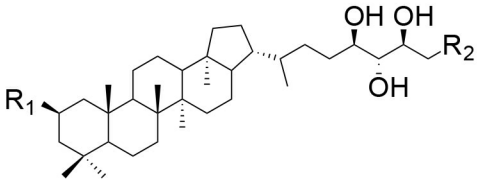

bacteriohopane aminotriol R_1 = H, R_2 = NH_2

bacteriohopanetetrol (BHT) R_1 = H, R_2 = OH

2Me-BHT R_1 = CH_3, R_2 = OH

BHT-glucosamine R_1 = H, R_2 =

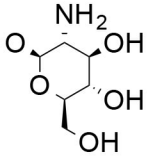

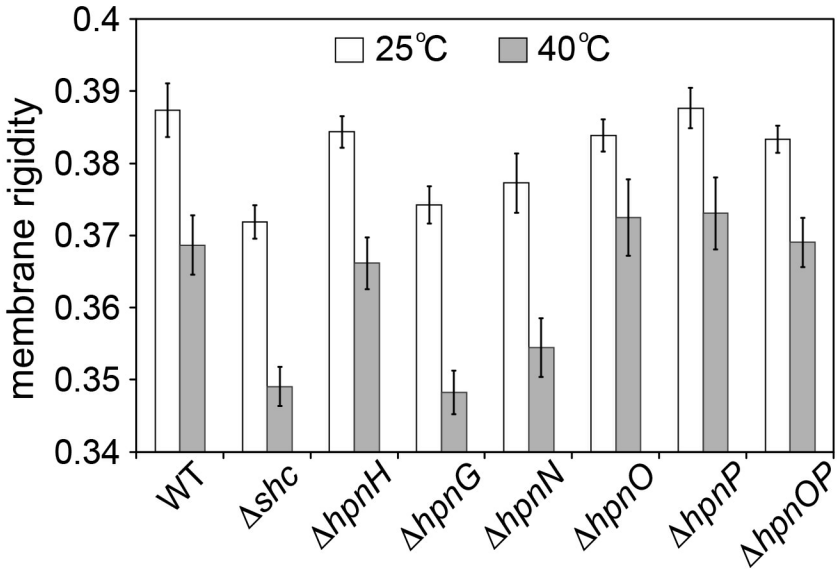
0.4
0.39
0.38
0.37
0.36
0.35
0.34
membrane rigidity
25℃
40℃
WT
Δshc
ΔhpnH
ΔhpnG
ΔhpnN
ΔhpnO
ΔhpnP
ΔhpnOP

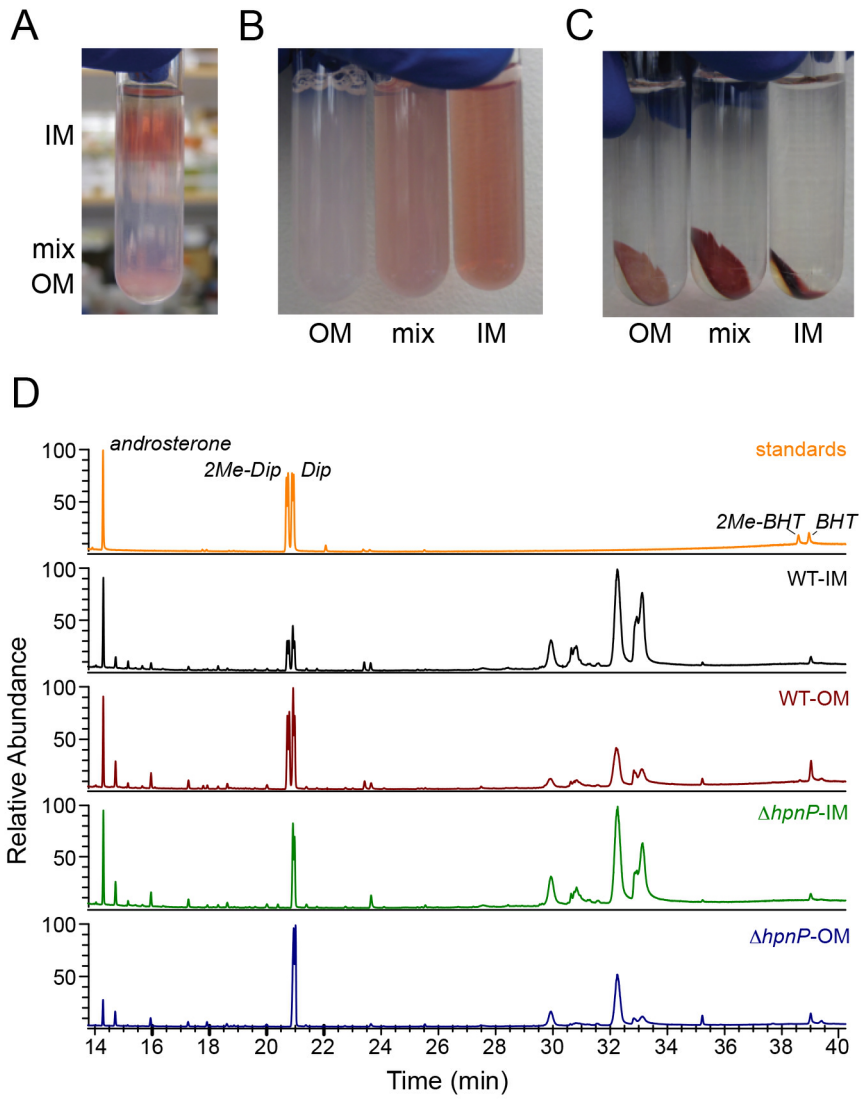
A
IM
mix
OM
B
OM
mix
IM
C
OM
mix
IM
D
androsterone
2Me-Dip
Dip
standards
2Me-BHT
BHT
WT-IM
WT-OM
ΔhpnP-IM
ΔhpnP-OM
Relative Abundance
100
50
14
16
18
20
22
24
26
28
30
32
34
36
38
40
Time (min)

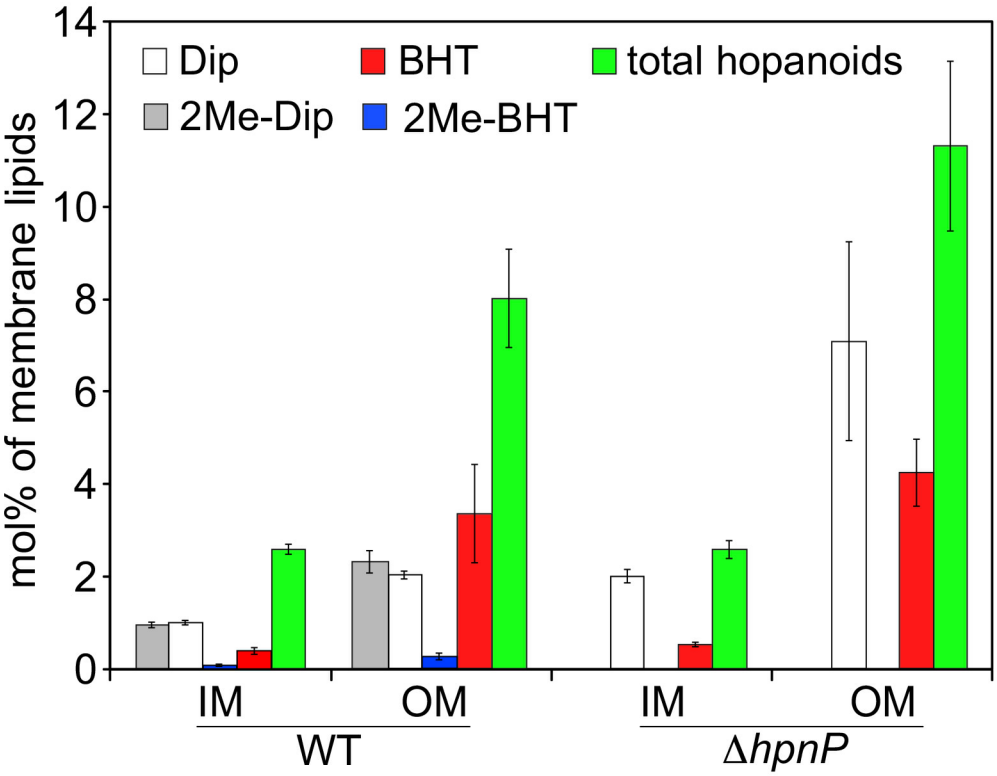
mol% of membrane lipids
14
12
10
8
6
4
2
0
Dip
BHT
total hopanoids
2Me-Dip
2Me-BHT
IM
OM
IM
OM
WT
ΔhpnP

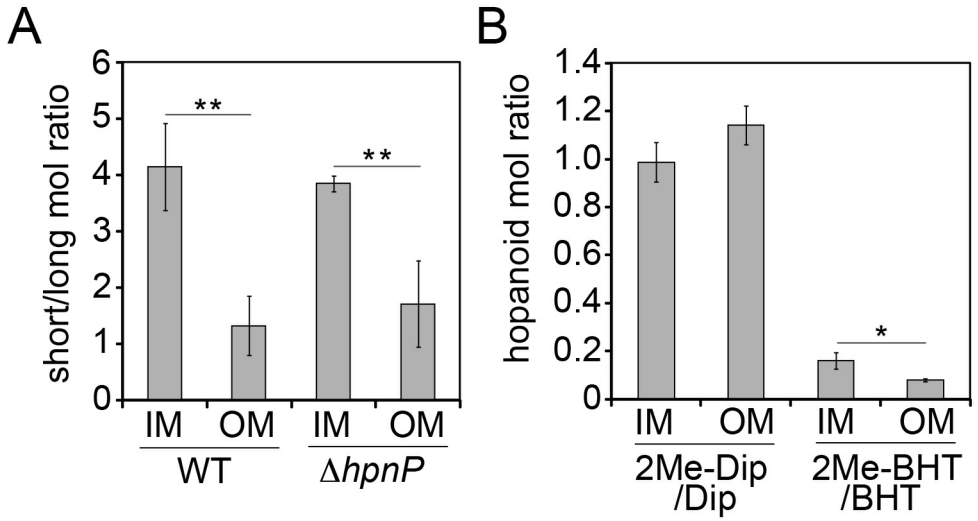
A
short/long mol ratio
6
5
4
3
2
1
0
**
**
IM
OM
IM
OM
WT
ΔhpnP
B
hopanoid mol ratio
1.4
1.2
1.0
0.8
0.6
0.4
0.2
0
*
IM
OM
IM
OM
2Me-Dip
/Dip
2Me-BHT
/BHT

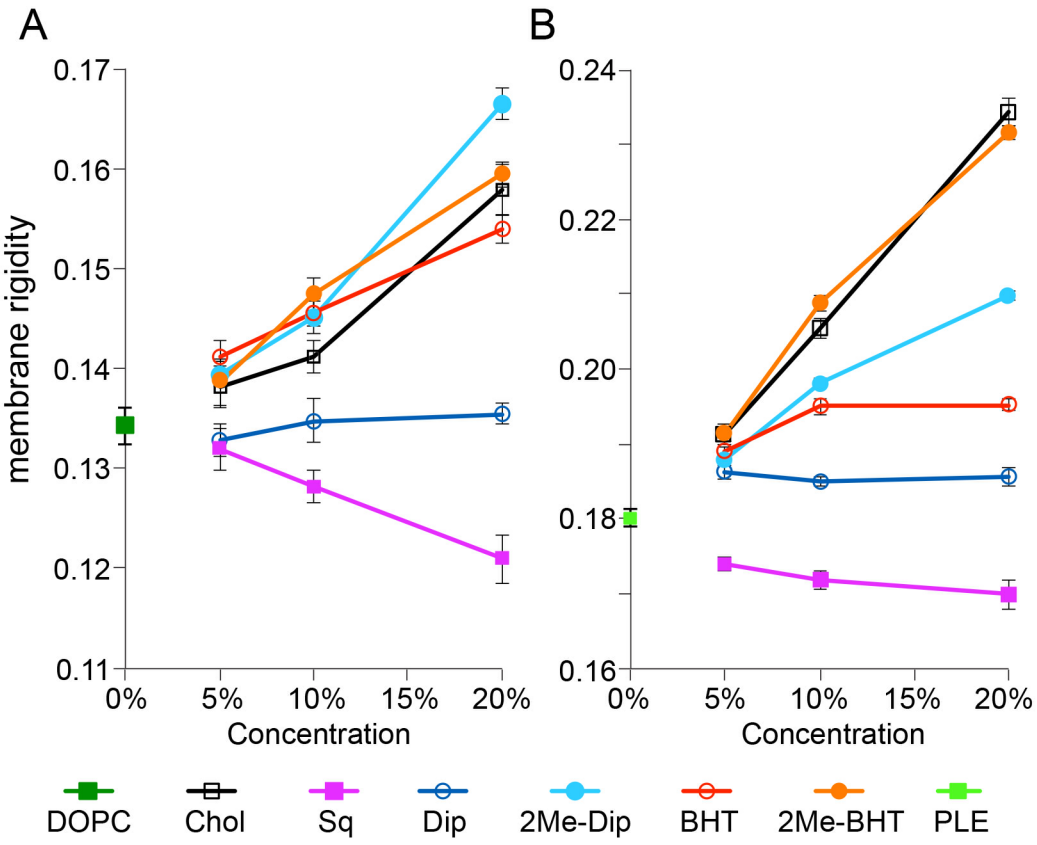
A
B
membrane rigidity
0.17
0.16
0.15
0.14
0.13
0.12
0.11
0.24
0.22
0.20
0.18
0.16
0%
5%
10%
15%
20%
Concentration
DOPC
Chol
Sq
Dip
2Me-Dip
BHT
2Me-BHT
PLE

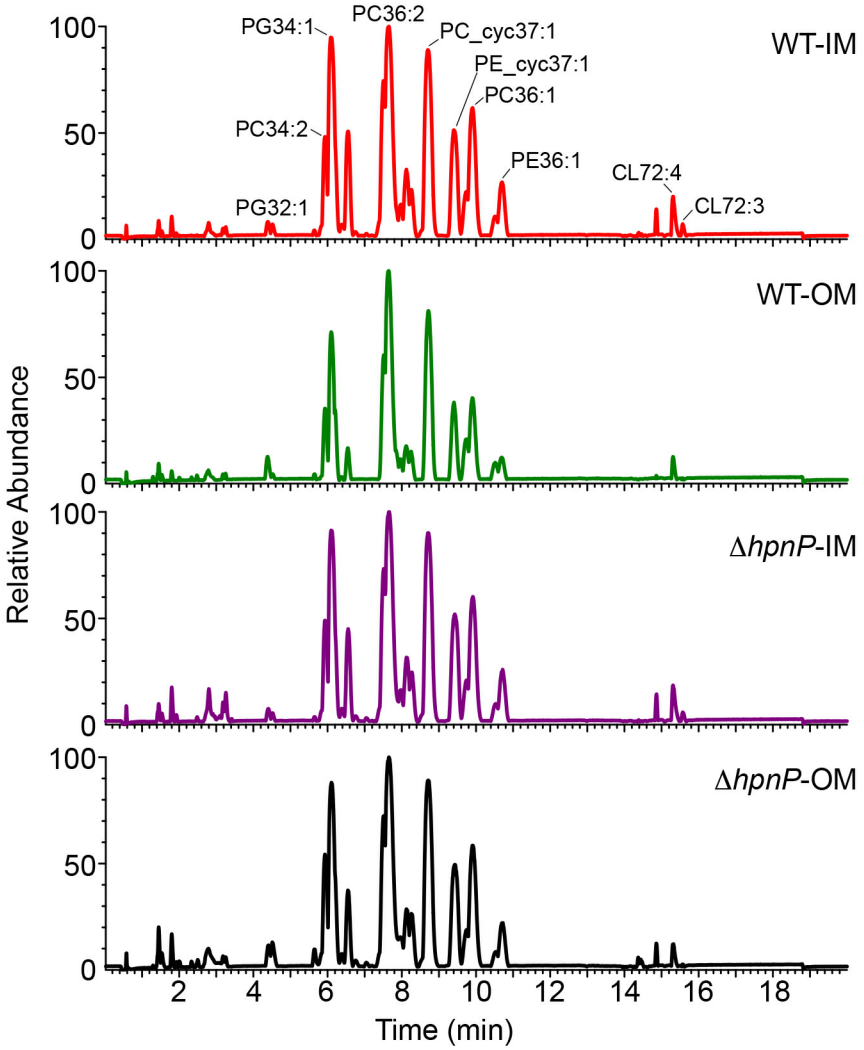
PG34:1
PC36:2
PC_cyc37:1
PE_cyc37:1
PC36:1
PC34:2
PE36:1
CL72:4
PG32:1
CL72:3
WT-IM
WT-OM
ΔhpnP-IM
ΔhpnP-OM
Relative Abundance
Time (min)
100
50
0
2
4
6
8
10
12
14
16
18

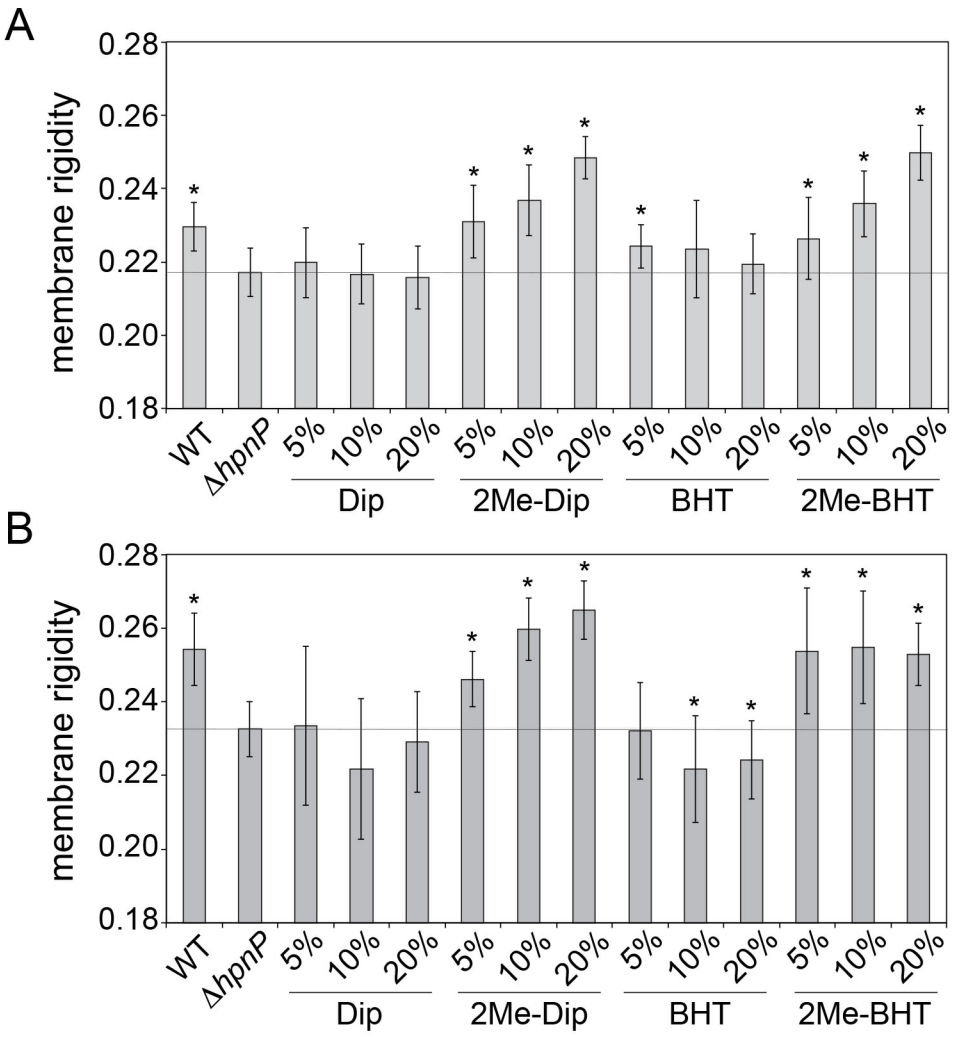
A
membrane rigidity
0.28
0.26
0.24
0.22
0.20
0.18
WT
ΔhpnP
5%
10%
20%
Dip
2Me-Dip
BHT
2Me-BHT
B
membrane rigidity
0.28
0.26
0.24
0.22
0.20
0.18
WT
ΔhpnP
5%
10%
20%
Dip
2Me-Dip
BHT
2Me-BHT